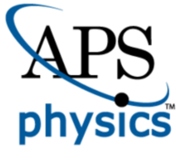

CHORUS

This is the accepted manuscript made available via CHORUS. The article has been published as:

Quantum gates with donors in germanium

Giuseppe Pica and Brendon W. Lovett

Phys. Rev. B **94**, 205309 — Published 29 November 2016

DOI: 10.1103/PhysRevB.94.205309

Quantum gates with donors in germanium

Giuseppe Pica[1,2] and Brendon W. Lovett[1]
[1]*SUPA, School of Physics and Astronomy, University of St Andrews, KY16 9SS, United Kingdom*
[2]*Center for Neuroscience and Cognitive Systems @UniTn,*
Istituto Italiano di Tecnologia, Corso Bettini 31 - 38068 Rovereto, Italy

Recent work has shown that electron spins in germanium (Ge) nanoscale transistors can be electrically tuned and have encouraging coherence times. Based on a novel, complete and validated theory of Ge-donor electron states, we propose that Ge spin qubits could have significant advantages over silicon (Si) in the implementation of a donor-based quantum processor architecture. Our work shows that the intrinsic features of the Ge band structure allow for a speedup of selective (local) one-qubit gates of up to two orders of magnitude as compared to Si. Further, we find that fast, robust two-qubit gates in Ge pose less stringent fabrication constraints than in Si devices: Ge-donors spaced three times farther apart than in Si show comparable exchange couplings, allowing more space for readout and control gates. In addition, for realistic position uncertainty in donor placement, Ge:P spin couplings have a 33% chance of being within an order of magnitude of the largest coupling, compared with only 10% in Si:P. It is therefore possible that a Ge based platform would enable fast, parallel and robust architectures for quantum computing.

I. INTRODUCTION

There has been astonishing progress in silicon (Si)-based spin quantum computing research[1], including demonstrated record coherence in the solid state[2,3]. However, the intrinsically weak spin-orbit interaction of the conduction electrons with the host Si nuclei[4] and the relative short range of the wave functions of the donor electrons[5] seriously restrict the speed of selective qubit control. Two-qubit gates in Si pose even greater challenges: Coupling two donor spins in Si requires the ions to be implanted very closely[6], and with high precision[7].

While retaining compatibility with integrated circuits, both theory[8,9] and experiments[10] have shown that spins in germanium (Ge)-heterostructures can be efficiently controlled electrically. Despite this decreased spin isolation, recent electron spin resonance (ESR) measurements of isotopically-purified-Ge donors have shown promising coherence times $T_2 \sim$ms[11]. Further, Ge has been considered as a candidate host for transistor processing in the quantum regime[12], and the technical development in device fabrication parallels the more established Si electronics[13,14].

Inspired by the recent progress, in this Letter we provide a thorough description of shallow Ge-donors from group V, based on an improved multi-valley effective mass theory (MV-EMT) that includes the strong anisotropy of the conduction band and approximates phenomenologically the interaction between the donor electron and the nucleus[5,15]. Our aim is to predict whether and by how much this new semiconductor platform could improve and facilitate single and two donor quantum gate operations.

We will first model DC gate control of the spin resonance frequency of donors[6,16,17], by calculating the Stark-shifted ESR spectrum: Close agreement with the experimental measurements of Ge:As performed concurrently with our theory and described in Ref. 18 validates our estimates. We will show that single qubit gates with Ge:P donors could be performed with nanosecond timescales under realistic assumptions: the corresponding 1000-fold speedup over the current state of the art in Si would enable a 150-fold reduction in qubit resources needed for fully error-corrected computing[19].

We will further calculate the exchange couplings J between adjacent Ge-donor spins, and quantify how their larger wave functions allow the stringent pitch requirements for Si-donors' placement to be relaxed by a factor of around three. Remarkably, we show that, in the optimal geometric configuration, J couplings between pairs of Ge-donors will depend less than those in Si on realistic 3D implantation misplacements. Uniform control of large, strongly coupled qubit clusters thus promises to be significantly easier in Ge, in spite of the ubiquitous problems of spin coupling intrinsic to multi-valley semiconductors[7,20,21].

II. DONOR ELECTRONS IN GE

The lowest conduction band in Ge has four equivalent minima (valleys) $\mathbf{k}_{0\mu}$, each located at the edge of the Brillouin zone along one of the equivalent crystallographic $\langle 111 \rangle$ directions in k space, the so-called L points[22]. The four-fold degeneracy of the ground state of a conduction electron in the undoped Ge crystal is lifted when a substitutional atom from group V is implanted. MV-EMT maintains that the donor quantum states can still be expanded in terms of packets of Bloch functions whose $\mathbf{k}$-vectors concentrate around each valley, since the wave function is known to spread across tens of lattice constants in space. When combined with a pseudopotential approach[5,15], it enables a reliable picture of the donor electron outside of the crystal cell occupied by the binding substitutional impurity (the *central cell*) to be obtained. This framework is perfectly suited to our goals: Both single and two-qubit manipulations of donor spins rely on the long-range behavior of the donor wave function.

The final MV-EMT equations that we are going to use

describe: i) the Bloch-expansion of the donor wavefunction,

$$\Psi(\mathbf{r}) \equiv \sum_\mu \alpha_\mu \xi_\mu(\mathbf{r}) \quad (1)$$
$$= \sum_\mu \alpha_\mu \frac{1}{(2\pi)^3} \int \tilde{F}_\mu(\mathbf{k}_\mu + \mathbf{k}_{0\mu}) \phi_0(\mathbf{k}_\mu + \mathbf{k}_{0\mu}, \mathbf{r}) d\mathbf{k}_\mu,$$

where we have conveniently defined ξ_μ as the total contribution of each envelope $\tilde{F}_\mu$ of Bloch functions $\phi_0(\mathbf{k}, \mathbf{r}) \equiv u_0(\mathbf{k}, \mathbf{r}) e^{i\mathbf{k}\cdot\mathbf{r}}$, centered at $\mathbf{k}_{0\mu}$, and α_μ are valley coefficients; ii) the expectation value of the Schrödinger equation defined by the bulk Hamiltonian H_0, solved by each eigenstate $\Psi(\mathbf{r})$ with eigenvalue ϵ,

$$\int d\mathbf{r} \sum_{\mathbf{G}} \sum_\mu \alpha_\mu^* F_\mu^*(\mathbf{r}) \times [\alpha_\mu (\mathbf{p} \cdot \mathbf{A}_\mu \cdot \mathbf{p} - \epsilon) F_\mu(\mathbf{r}) + \quad (2)$$
$$\sum_\nu \alpha_\nu e^{-i(\mathbf{k}_{0\mu} - \mathbf{k}_{0\nu})\cdot\mathbf{r}} C_{\mathbf{G}}(\mathbf{k}_{0\nu}, \mathbf{k}_{0\mu}) e^{i\mathbf{G}\cdot\mathbf{r}} U(\mathbf{r}) F_\nu(\mathbf{r})] = 0,$$

where the labels μ and ν each run across the four valley minima, $\mathbf{p} \cdot \mathbf{A}_\mu \cdot \mathbf{p}$ is the anisotropic kinetic energy operator for the μ valley, $U(\mathbf{r})$ is the impurity potential, $\sum_{\mathbf{G}} C_{\mathbf{G}}(\mathbf{k}, \mathbf{k}') e^{i\mathbf{G}\cdot\mathbf{r}} \equiv u_0^*(\mathbf{k}, \mathbf{r}) u_0(\mathbf{k}', \mathbf{r})$ is the expansion of the lattice-periodic portion of the Bloch functions in terms of the vectors $\{\mathbf{G}\}$ of the Ge reciprocal lattice, and $F_\mu(\mathbf{r})$ are the Fourier transformed envelopes. Full details of how this MV-EMT equation is derived from the exact Schrödinger equation of the donor electron, and the approximations entailed therein, can be found in Appendix A. An important further improvement to most of the previous EMT approaches is to include the full Bloch structure of the donor states: we use the weights $C_{\mathbf{G}}(\mathbf{k}_{0\mu}, \mathbf{k}_{0\nu})$ as evaluated in Ref. 23 after a pseudopotential calculation of the band structure of the undoped Ge crystal[24].

A pseudopotential method is employed to describe the impurity potential $U(\mathbf{r})$, an approach that has been successfully applied to understanding properties of donor electron states in Si[5]. We require a phenomenological pseudopotential that takes the simplest possible form while enabling a unified and accurate description of all group V donors, which matches both the experimental binding energies and the hyperfine interactions of the impurity ion. The following short-ranged pseudopotential with spherical symmetry:

$$U(\mathbf{r}) = -\frac{e^2}{\epsilon_{\mathrm{Ge}}|\mathbf{r}|}(1 - \mathrm{e}^{-b|\mathbf{r}|} + B|\mathbf{r}|\mathrm{e}^{-b|\mathbf{r}|}) \equiv -\frac{e^2}{\epsilon_{\mathrm{Ge}}|\mathbf{r}|} + U_{cc}(\mathbf{r}), \quad (3)$$

meets our needs[5,15]. Here, $\epsilon_{\mathrm{Ge}} = 16.2$ is the static dielectric constant for Ge, e is the elementary charge, and b and B are two donor-dependent parameters.

We solve our MV-EMT equation variationally: once two values for b and B are chosen, trial envelopes F_μ^0 that reproduce the anisotropic symmetry of each valley are optimized to minimize the expectation value of the energy over the corresponding state. If we consider for example the $[111]$ valley, and orient the spatial $\{x, y, z\}$ Cartesian axes along $\{[1\bar{2}1], [10\bar{1}], [111]\}$ respectively, we follow Ref. [5] to write our *ansatz* as:

$$F_{111}^0(x, y, z) = N_0 \left[\mathrm{e}^{-\sqrt{\frac{x^2+y^2}{a_s^2} + \frac{z^2}{b_s^2}}} + \beta\, \mathrm{e}^{-\sqrt{\frac{x^2+y^2}{a_l^2} + \frac{z^2}{b_l^2}}} \right]. \quad (4)$$

Here, N_0 is a suitable normalization that implies $\int_{\text{all space}} d\mathbf{r}\, |F_{111}^0(\mathbf{r})|^2 = 1$, while the other coefficients are five variational parameters. The optimal values of our variational solutions for $\Psi(\mathbf{r})$, alongside the best pseudopotential parameters that describe the ion-electron interaction throughout the rest of the paper, are listed in Appendix B.

Following our analogous treatment of the Stark effect for donors in Si[5], we next alter the trial envelopes (Eq. (4)) to account for the modifications that the ground wave function undergoes as a result of a uniform electric field that is turned on externally[25]: $H = H_0 - e\mathbf{E} \cdot \mathbf{r}$. Each envelope changes depending on the direction of the field relative to the principal axis of its effective mass tensor. We thus use an extra variational coefficient for each envelope, that describes how the envelope elongates in the field direction[25]. For illustration, if we define $\{x, y, z\}$ Cartesian axes along $\{[1\bar{2}1], [10\bar{1}], [111]\}$, we extend our zero-field *ansatz* (Eq.4) for the $[111]$ envelope to

$$F_{111} = N \left[\mathrm{e}^{-\sqrt{\frac{x^2+y^2}{a_s^2} + \frac{z^2}{b_s^2}}} + \beta\, \mathrm{e}^{-\sqrt{\frac{x^2+y^2}{a_{l,\hat{\mathbf{E}}}^2} + \frac{z^2}{b_{l,\hat{\mathbf{E}}}^2}}} \right] \times$$
$$\times (1 + q(\mathbf{E}) \hat{\mathbf{E}} \cdot \mathbf{r}), \quad (5)$$

where $q(\mathbf{E})$ is a variational parameter describing the elongation along the field direction $\hat{\mathbf{E}}$ and the long range lengths $a_{l,\hat{\mathbf{E}}}$ and $b_{l,\hat{\mathbf{E}}}$ are further allowed to change from their zero-field values[25] (see also Appendix F where we check our results using a larger variational basis). We remark that different envelopes will have different optimal elongations. With no further introduction of adjustable parts in our bulk pseudopotential, the expectation value of the energy is again minimized over the complete singlet A_1 ground state, as a function of the electric field vector $\mathbf{E}$.

The angle of the applied field determines the degree to which the leftover bulk symmetry of the crystal is broken, and different angles lead to very different valley redistributions within the ground state: $\mathbf{E} \parallel \langle 100 \rangle$ forms equal angles with all valleys, so the energy spectrum is only rigidly shifted from the zero-field configuration, and the valley weights are not reorganized. At the opposite extreme, if $\mathbf{E} \parallel [111]$, the field orientation induces a maximal repopulation of the $[111]$ valley (a) with respect to the other three valleys (m). In Appendix C, we prove that this repopulation is approximately equal to

$$\gamma_G(\mathbf{E}) \equiv 2[\alpha_a(\mathbf{E}) - \alpha_m(\mathbf{E})] \approx -\frac{1}{4} \frac{\Lambda_m(\mathbf{E}) - \Lambda_a(\mathbf{E})}{\Delta_0}, \quad (6)$$

where $\Lambda_{a(m)}$ are the valley diagonal energies for the $m(a)$ valleys, and Δ_0 is the bulk inter-valley coupling. A similar equation holds for Stark-shifted donors in silicon (with a different proportionality constant), and direct comparison of

the two cases shows that γ_G is about one order of magnitude larger in Ge than in Si, as a result of a weaker valley-orbit interaction Δ_0.

III. SINGLE-QUBIT GATES

The valley population for Ge donor wave functions in electric fields has important consequences for the operation of quantum gates with Ge donors: Such local electrostatic distortions affect the donor spin resonance spectrum by tuning both the contact hyperfine coupling $A\mathbf{I}\cdot\mathbf{S}$ between the nuclear spin I and the electron spin S, and the **g**-tensor that modulates the Zeeman interaction of the electron spin with an external magnetic field. Controlling this tuning provides a natural way to achieve qubit selective manipulation and the degree of tuning sets upper bounds on gate speeds[6]. This has been thouroughly charted for Si donors[16,17,26–28]; we now explore what could be achieved in Ge.

In Appendix C we show that no speedup comes from hyperfine-Stark shifted donors from Si to Ge. However, the g-factor electrical tuning is much more promising: The spin-orbit interaction of conduction electrons with the host Ge nuclei is strong enough that the bulk g-factor $g_0 = 1.57$ differs markedly from the free electron value $g \sim 2$. Owing to the large mass anisotropy of the Ge conduction band, each valley axis $\hat{\mu}$ displays two distinct g-tensor components depending on whether $\mathbf{B}$ is parallel ($g_\parallel$) or perpendicular ($g_\perp$) to it: $g_\perp - g_\parallel \approx 1.05$, which is three-orders-of-magnitude larger than the corresponding Si value. It follows that the effective electrically-induced valley repopulation described in Eq. 6 can offer a powerful tuning mechanism if the giant anisotropy of the Ge valleys' g-factors is combined to maximal effect. The optimal configuration, as described above, corresponds to $\mathbf{E} \parallel \langle 111\rangle$. The anistropy of the g tensor means that different directions of the applied magnetic field $\mathbf{B}_0$ will yield different values of the Zeeman splitting. For example, if $\mathbf{B}_0 \parallel \langle 111\rangle$, the magnitude of the g-factor is $g(\mathbf{E}) = g_0 + 2\Delta_g(\mathbf{E})$, while if $\mathbf{B}_0 \perp \langle 111\rangle$ then $g(\mathbf{E}) = g_0 - \Delta_g(\mathbf{E})$, where

$$\Delta_g(\mathbf{E}) \equiv \frac{g_\parallel - g_\perp}{3}(\gamma_G^2 - 1)/(3 + \gamma_G^2) \tag{7}$$

(see Appendix C) is a measure of the orientational dependence. Remarkably, the detuning $(g(\mathbf{E}) - g_0)\mu_\mathrm{B} B_0$ (where μ_B is the Bohr magneton) can be very large even for modest magnetic fields: Fig. 1 shows a density plot of the detuning of a Ge:P bulk spin with $\mathbf{E} \parallel \langle 111\rangle$ and $B_0 = 0.4$ T (corresponding to $T_2 \approx 1$ ms as measured in Ref. 11) as a function of the electric field magnitude and the angle between $\mathbf{E}$ and $\mathbf{B}_0$. Strikingly, we show that qubit detunings of over 1 GHz could be attained within a realistic experimental setting, thus allowing for nanosecond selective resonant manipulation – a two-orders-of-magnitude improvement on any maximum speed achievable with detuned Si donor spins[5].

We are able to completely characterize the g-factor tunabilities of all donors (for details see Appendix C), and these agree quantitatively with recent measurements in Ref. 18 of Ge:P and Ge:As. This validates our theory and builds our confidence in all the results presented in this Letter.

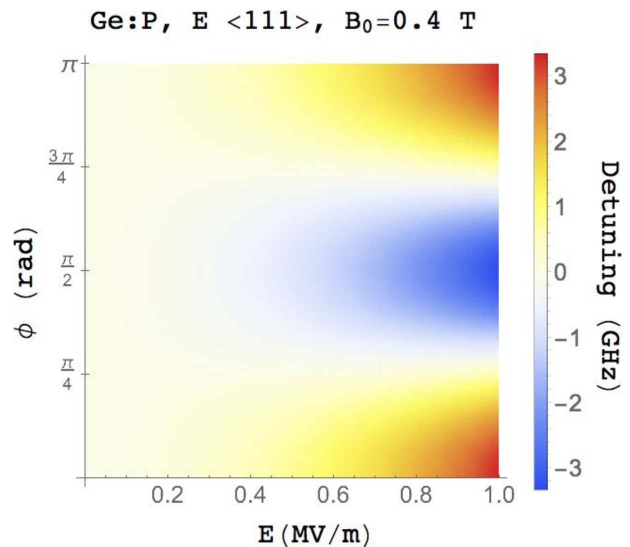

FIG. 1: Density plot of the Stark-detuned Zeeman coupling $[g(E) - g_0]\mu_\mathrm{B} B_0$ induced by a nonzero electric field $\mathbf{E}$, aligned with the $\langle 111\rangle$ crystallographic direction, with an angle ϕ between $\mathbf{E}$ and the magnetic field $\mathbf{B}_0$. For realistic applied voltages, the detuning can be changed over the range $\{-3$ GHz, 3 GHz$\}$, allowing for nanosecond selective manipulation of locally detuned spins. $B_0 = 0.4$ T corresponds to a donor spin coherence $T_2 \approx 1$ ms[11].

Two-qubit gates The exchange interaction J between neighboring electron spins with overlapping orbital densities provides the most natural spin qubit coupling in semiconductor architectures[6,29]. To assess the promise of Ge donor spin qubits, it is critical to understand how large these spin couplings can be, and how robust they are against fabrication errors.

Exchange couplings J in multivalley semiconductors can be reliably evaluated within the Heitler-London approach[30], for the regime required for quantum gates[5,7,31,32] (see Appendix E). It is well known that J oscillates with donor separation $\mathbf{d}$ with a period of order the crystal lattice constant. Practical implementation of two-qubit operations must then be robust to the large range of coupling magnitudes that then results from an ensemble of qubits with different donor separations $\mathbf{d}$, since state-of-the-art donor placement is limited to precision of a few nm[33–35]: this is arguably the most significant hurdle to large-scale quantum computing in silicon.

Based on the Ge:P wavefunction calculated here, and the Si:P wavefunction calculated in our previous work[5], we set to model a statistical ensemble of donor pairs, whose separation vectors $\mathbf{d}$ are combinations of the same nominal distance $\mathbf{d}_0$ and a random vector $\mathbf{d}_r$ that is uniformly distributed in a cube with edge length of 5 nm (see insets of Fig. 2). This scenario is compatible with the imprecision in donor positioning of modern ion implantation methods[36] used to fabricate semiconductor nanodevices for quantum computing.

Owing to the peculiar band structure in Ge, we find that

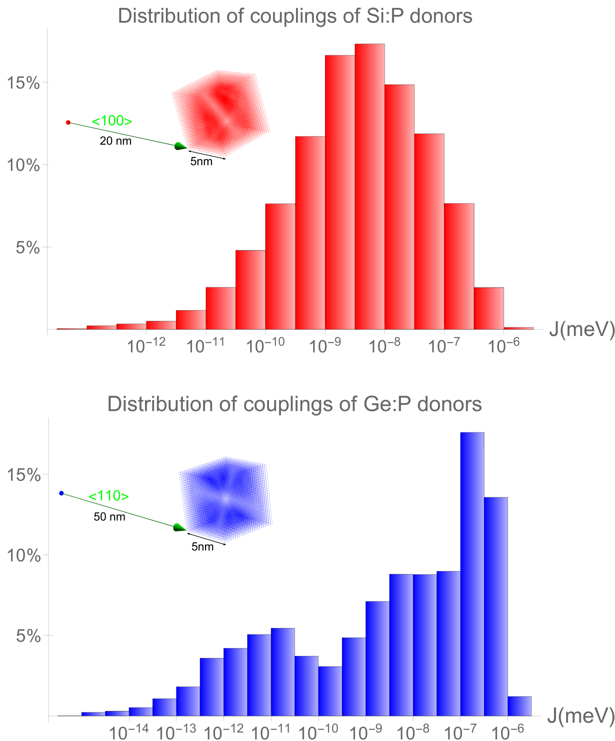

FIG. 2: Distribution of J couplings (on a log-scale) of a statistical ensemble of Si:P (top) and Ge:P (bottom) donor pairs, with pair separations $\mathbf{d}_0 + \mathbf{d}_r$, where the nominal separations are $\mathbf{d}_0^{\text{Si}} = [20\text{ nm}, 0, 0]$, $\mathbf{d}_0^{\text{Ge}} = [50/\sqrt{2}\text{ nm}, 50/\sqrt{2}\text{ nm}, 0]$ for Si and Ge respectively. These combine with a random separation $\mathbf{d}_r$ that is uniformly distributed over cubes with edge length 5 nm. These cubes are illustrated in the insets and show all the possible positions of donors partners that could couple to a fixed donor at the origin of the $\mathbf{d}_0$ vector. The Ge:P distribution spreads across more orders of magnitude overall, but it is more skewed towards larger couplings.

aiming for $\mathbf{d}_0 \parallel \langle 110 \rangle$ gives the minimal spread possible in the distribution of J couplings of a Ge-donor ensemble (see Appendix D). The optimal choice for Si:P is known to be $\mathbf{d}_0 \parallel \langle 100 \rangle$[21]. The corresponding ensembles of J couplings are distributed as shown in Fig. 2. For fair comparison, we set similar mean couplings in Ge and Si - it is here 3.5×10^{-9} meV in the Si:P cluster and 3×10^{-9} meV in the Ge:P cluster, corresponding to an average donor separation that increases from 20 nm in Si:P to 50 nm in Ge:P. From the fabrication point of view, this feature already promises a significant relative improvement, as the more relaxed lengthscales in Ge would directly allow for much more space between donors for control gates and readout devices.

The distribution of J couplings for Ge:P donors is clearly more skewed towards higher coupling values than it is for Si:P: Larger couplings are more appealing as they imply the possibility of faster gates that are more robust against single-qubit decoherence. A more complete comparison is presented in Fig. 3, where cumulative distributions of the coupling ensembles from Si:P and Ge:P are shown on top of one another. After ion implantation, it is reasonable to assume that device characterization should identify the donors that are best suited for hosting quantum information: current

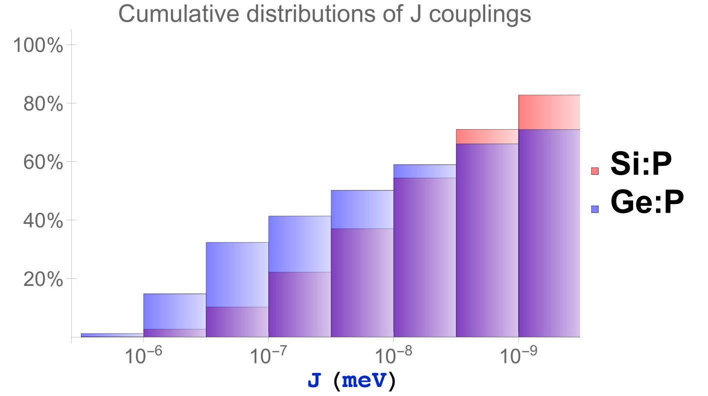

FIG. 3: Comparison of the cumulative distributions of the ensembles of Ge:P and Si:P couplings (on a log-scale) across the top four orders of magnitude of J. As explained in the text, the larger skew of the Ge:P distribution in Fig. 2 implies higher probabilities for Ge:P couplings to lie within the top two orders of magnitude. Larger couplings are desirable for faster two-qubit gates, and current schemes for uniform control of such gates in a cluster require that J values vary at most within two orders of magnitude in the cluster. In this sense, Ge:P donors provide a significant advantage over Si:P.

schemes for exchange-based two-qubit gates[37,38] require that the range of J couplings is contained within about two orders of magnitude, if the same kind of control is to be used across the device (or the cluster). Fig. 3 shows that, with the same donor positioning imprecision, there is a 33% chance of a Ge:P pair yielding a coupling within one order of magnitude from the strongest in the set, while this probability drops to less than 11% for Si:P pairs. This advantage remains, albeit diminished, even if the chosen implementation architecture is robust to more than two orders of magnitude in J (it is currently hard to imagine, however, how uniform control could be extended to clusters with more than two orders of magnitude variations of J). These considerations do not change if other sets of donor distances are considered: decreasing $\mathbf{d}_0$ just leads to an exponential gain in J (see SM), thus the relative ratios of the J couplings within each cluster to their mean value are not changed. Thus, the requirements on precise donor positioning would be significantly less demanding for Ge:P than for Si:P donors.

IV. CONCLUSIONS

Starting from a complete theory of shallow Ge-donors, based on an improved MV-EMT with full inclusion of the Bloch states' structure, we have assessed aspects of the performance of both single and two-qubit operations with donor spins in Ge. Close agreement with recent experiments[18] validates our predictions.

The giant tunability of the Zeeman splittings of Ge-donors suggests that nanosecond selective electrical spin manipulation could be achieved within realistic experimental settings. Further, the same average spin exchange coupling between two Si:P donors could be achieved with two Ge:P

donors almost three times farther apart, which promises much more space for fabricating control gates and readout devices in heterostructures. Finally, in the optimal geometric configuration we show that the relative variation of the J coupling across a realistic ensemble of randomly misplaced donors is smaller in Ge than in Si, which would make uniform control of large qubit clusters relatively easier. Future improvements in implantation accuracy that will increase the yield of working qubits could thus enable efficient surface codes faster in Ge than in Si[39].

With millisecond spin coherence times recently demonstrated by Ge-donor spins[11], and with fast developing spin transport in Ge heterostructures[40], Ge is already close to matching several requirements for quantum computing. Our calculations show that Ge is a very promising alternative to the more established Si framework, and should inspire further experimental investigations.

Acknowledgments

We wish to thank Stephen Lyon and Anthony Sigillito for drawing our attention to the problem of describing donor states in Ge and for sharing their experimental data with us. This research was funded by the joint EPSRC (EP/I035536)/ NSF (DMR-1107606) Materials World Network grant (GP, BWL), the EPSRC grant EP/K025562 (BWL). GP thanks the University of St Andrews and the EPSRC for a Doctoral Prize Fellowship.

Appendix A: Multi-valley effective mass theory of donors in germanium

Extensive ESR experiments with Ge:P, Ge:As and Ge:Bi donors at low temperature were already performed by Wilson[41] as far back as the ’60s. However, the theoretical understanding of Ge donors is still not well developed: the most modern approaches to describing the electron orbital states date back to the ’70s[23,42,43], with a satisfactory theory still missing to date. As explained in the main text, we attack this problem using effective mass theory, because it gives a satisfactory description of the long-range component of the donor electron donor probability densities, which is all that is needed for predicting the features of single and two-qubit gates, while at the same time keeping the theoretical framework light enough that those features can be flexibly evaluated within different realistic environments.

Over the years, EMT has been improved from its original single-valley formulation[44,45] to a multi-valley framework[5,15,20,46–49], which aims to describe how the valleys are admixed in the electron eigenstates as a result of the donor-dependent impurity potential $U(\mathbf{r})$. The most important consequences for the electron ground state are that it is non-degenerate, and its orbital energy and hyperfine coupling to the ion differ significantly from a single-valley state[41,50]. As compared to Si-donors, electron wave functions in Ge are more spread out because of both stronger dielectric screening from the crystal and smaller average effective mass of the lowest conduction band. This is evident if one compares the rescaled effective Rydberg energies and transverse Bohr radii of the orbital states in Si ($a^*_{Si} = \hbar^2\epsilon_{Si}/(m^*_{\perp,Si}e^2) = 3.157$ nm, $Ry^* = m^*_{\perp,Si}e^4/2\hbar^2\epsilon^2_{Si} = 19.98$ meV) and Ge ($a^*_{\mathrm{Ge}} = 10.244$ nm, $Ry^* = 4.45$ meV).

We now present the most important steps that lead to the final MV-EMT equation that is used in the main text (Eq. 2), starting from the exact Schrödinger equation for a donor electron in bulk Ge:

$$H^0\Psi(\mathbf{r}) = \left[-\frac{\hbar^2}{2m_0}\nabla^2 + V^0(\mathbf{r}) + U(\mathbf{r})\right]\Psi(\mathbf{r}) = \epsilon\Psi(\mathbf{r}), \tag{A1}$$

where $\Psi(\mathbf{r})$ is the wave function of the donor electron, m_0 is its rest mass, $V^0(\mathbf{r})$ is the periodic potential of the undoped Ge crystal, and ϵ labels any energy eigenvalue.

EMT dictates that $\Psi(\mathbf{r})$ be expanded as a sum of the Bloch functions of the conduction electrons in undoped Ge $\phi_0(\mathbf{k},\mathbf{r}) \equiv u_0(\mathbf{k},\mathbf{r})e^{i\mathbf{k}\cdot\mathbf{r}}$, each weighted with envelopes $\tilde{F}_\mu$ that decay rapidly as their argument gets farther from each of the four valleys $\mathbf{k}_{0\mu}$[44]: this corresponds to Eq (1) in the main text, which we repeat here for convenience:

$$\Psi(\mathbf{r}) \equiv \sum_\mu \alpha_\mu \xi_\mu(\mathbf{r}) = \sum_\mu \alpha_\mu \frac{1}{(2\pi)^3}\int \tilde{F}_\mu(\mathbf{k}_\mu + \mathbf{k}_{0\mu})\phi_0(\mathbf{k}_\mu + \mathbf{k}_{0\mu},\mathbf{r})d\mathbf{k}_\mu, \tag{A2}$$

where we have conveniently defined ξ_μ as the total contribution of each envelope centered at $\mathbf{k}_{0\mu}$, and α_μ are valley coefficients that can be predicted by symmetry arguments alone[41]. In fact, the four-fold $1s$ valley manifold can be grouped into a singlet A_1 and a triplet T_2:

$$\alpha_i(A_1) = \tfrac{1}{2}(1,1,1,1)$$
$$\alpha_i(T_2) = \begin{cases} \frac{1}{\sqrt{2}}(1,-1,0,0) \\ \frac{1}{2}(1,1,-1,-1) \\ \frac{1}{\sqrt{2}}(0,0,1,-1). \end{cases} \tag{A3}$$

A further step of EMT is to encode the Hamiltonian of the pure crystal in an effective mass tensor specific to the lowest conduction band: this contributes an anisotropic kinetic energy operator $\mathbf{p}\cdot\mathbf{A}_\mu\cdot\mathbf{p}$ for each $\hat{\mu}$ valley. Here, $\mathbf{p}$ is the momentum operator of the donor electron, and $\mathbf{A}_\mu$ is a diagonal tensor in a basis with one vector parallel to $\hat{\mu}$ and two vectors orthogonal to it (e.g., if $\hat{\mu} \parallel [111]$, one could choose the basis $\{[1\bar{2}1],[10\bar{1}],[111]\}$), with entries $A^{11}_\mu = A^{22}_\mu = 1/(2m^*_\perp)$ and $A^{33}_\mu = 1/(2m^*_\parallel)$, where $m^*_\perp = 0.0815\ m_0$ and $m^*_\parallel = 1.59\ m_0$.

We are thus ready, following Ref. 47, to take the expectation values of both sides of Eq. (A1) for the wave function in Eq. (A2). After performing the $\mathbf{k}$ integrations and introducing the Fourier transformed envelopes $F_\mu(\mathbf{r})$, this gives Eq. II in

the main text:

$$\int d\mathbf{r} \sum_{\mathbf{G}} \sum_{\mu} \alpha_\mu^* F_\mu^*(\mathbf{r}) \times [\alpha_\mu(\mathbf{p}\cdot\mathbf{A}_\mu\cdot\mathbf{p}-\epsilon)F_\mu(\mathbf{r})+ \\ \sum_\nu \alpha_\nu e^{-i(\mathbf{k}_{0\mu}-\mathbf{k}_{0\nu})\cdot\mathbf{r}} C_{\mathbf{G}}(\mathbf{k}_{0\nu},\mathbf{k}_{0\mu}) e^{i\mathbf{G}\cdot\mathbf{r}} U(\mathbf{r}) F_\nu(\mathbf{r})] = 0, \tag{A4}$$

where the labels μ and ν each run across the four valley minima, and $\sum_{\mathbf{G}} C_{\mathbf{G}}(\mathbf{k},\mathbf{k}')e^{i\mathbf{G}\cdot\mathbf{r}} \equiv u_0^*(\mathbf{k},\mathbf{r})u_0(\mathbf{k}',\mathbf{r})$ is the expansion of the lattice-periodic portion of the Bloch functions in terms of the vectors $\{\mathbf{G}\}$ of the Ge reciprocal lattice. We have also assumed that $C_{\mathbf{G}}(\mathbf{k}_{0\mu}+\mathbf{k}_\mu, \mathbf{k}_{0\nu}+\mathbf{k}_\nu) \approx C_{\mathbf{G}}(\mathbf{k}_{0\mu},\mathbf{k}_{0\nu})$, as it is found that these weights vary weakly for small displacements of their arguments.

We combine this MV-EMT with a pseudopotential method to describe the impurity potential $U(\mathbf{r})$. The use of a smooth pseudopotential in place of the true impurity potential implies that the eigenstates of the corresponding Hamiltonian are not accurate on the scale of the central cell[15], where strong oscillations impede the semi-analytic description we are aiming at. However, the pseudo-wave function averages the short-ranged behaviour and matches it consistently with the more accurate picture farther from the nucleus. The past decades have seen a plethora of functional forms proposed for the impurity pseudopotential, whereby few adjustable parameters were tuned until the low-energy donor states matched one or more experimental binding energies. However, we recently pointed out that the variational solutions of the corresponding pseudo-Hamiltonians are not fundamentally granted to provide sensible descriptions of the donor *eigenstates* of the problem in Eq. (A1), although they can give reliable upper bounds to its exact *eigenvalues*[5,21]. Thus we suggested that, within an analytical MV-EMT and pseudopotential framework, the tunable parameters in $U(\mathbf{r})$ should also fit the hyperfine coupling to the impurity ion, in order to constrain the average short-ranged behaviour of the pseudo-state, and, crucially, to improve the description of the eigenstates. We require, then, a phenomenological pseudopotential which is the simplest possible that allows for a unified and accurate framework across all donors. As mentioned in the main paper, we use the following short-ranged pseudopotential with spherical symmetry:

$$U(\mathbf{r}) = -\frac{e^2}{\epsilon_{\text{Ge}}|\mathbf{r}|}(1-\mathrm{e}^{-b|\mathbf{r}|}+B|\mathbf{r}|\mathrm{e}^{-b|\mathbf{r}|}) \equiv -\frac{e^2}{\epsilon_{\text{Ge}}|\mathbf{r}|}+U_{cc}(\mathbf{r}). \tag{A5}$$

Here, $\epsilon_{\text{Ge}} = 16.2$ is the static dielectric constant for Ge, e is the elementary charge, and b and B are two donor-dependent parameters that will be fit, once for all, to the experimental binding energies and hyperfine coupling.

Unlike our previous work on Si donors in Ref. 5, we find that a consistent picture requires an important further improvement, as we now explain. Most of the previous EMT approaches go on to neglect the $\mathbf{G} \neq 0$ terms of the plane-wave expansion of the Bloch states $u_0(\mathbf{k},\mathbf{r})$[47], as they mostly multiply higher Fourier components of the impurity potential in Eq. (II). However, it is not always true that these terms are less important than the $\mathbf{G} = 0$ terms, and this approximation has been criticized[20,51]. The assumption is particularly questionable for Ge donors, since the most important Bloch states $u_0(\mathbf{k} \sim \mathbf{k}_{0\mu},\mathbf{r})$ in Eq. (A2) in Ge are even farther from $\mathbf{k} = 0$ than in Si. Thus, Umklapp scattering terms from the periodic lattice potential are more important, as it is easier for reciprocal lattice vectors $\mathbf{G}$ to 'resonantly' match differences $\mathbf{k}-\mathbf{k}'$ between two momenta belonging to separate Brillouin zones. The inter-valley weights $C_{\mathbf{G}}(\mathbf{k}_{0\nu},\mathbf{k}_{0\mu})$ ($\mu \neq \nu$) with $\mathbf{G} \neq 0$ are thus expected to be more significant, as direct pseudopotential calculations show[23,24].

$\mathbf{G}$ shell	$C_{\mathbf{G}}(\mathbf{k}_{0\mu},\mathbf{k}_{0\nu}), \mu \neq \nu$
$\langle 000 \rangle$	0.42
$\langle 111 \rangle$	0.35
$\langle 200 \rangle$	0.0
$\langle 220 \rangle$	0.95
$\langle 311 \rangle$	0.39

TABLE I: Intervalley coupling weights $C_{\mathbf{G}}(\mathbf{k}_{0\mu},\mathbf{k}_{0\nu})$ due to the crystal periodic parts of the Bloch functions pinned to any two different Ge valleys $\mu \neq \nu$, scanned at different $\mathbf{G}$ shells. Adapted from Ref. 23.

Our solution is to include the full Bloch structure of the donor states: the list of the relevant weights $C_{\mathbf{G}}(\mathbf{k}_{0\mu},\mathbf{k}_{0\nu})$ has been evaluated in Ref. 23 after a pseudopotential calculation of the band structure of the undoped Ge crystal[24]. We report the relevant results in Table I for convenience. Specifically, we neglect those terms that either have vanishing weights ($|C_{\mathbf{G}}(\mathbf{k}_{0\mu},\mathbf{k}_{0\nu})| \lesssim 0.1$) or that sample very high Fourier components $\tilde{U}(\mathbf{k}_{0\mu}-\mathbf{k}_{0\nu}-\mathbf{G} \gtrsim 4k_0)$ and are thus negligible. We verify *a posteriori* that the numerical results obtained here are not influenced significantly by these approximations.

Appendix B: Bulk $1s$ Ge-donor states

As pointed out in the main text, our variational solution of the MV-EMT equation (II) requires the choice of trial envelopes F_μ^0: as an example, if the spatial $\{x,y,z\}$ Cartesian axes are oriented along $\{[1\bar{2}1],[10\bar{1}],[111]\}$ respectively, we set

$$F_{111}^0(x,y,z) = N_0 \left[\mathrm{e}^{-\sqrt{\frac{x^2+y^2}{a_s^2}+\frac{z^2}{b_s^2}}} + \beta\,\mathrm{e}^{-\sqrt{\frac{x^2+y^2}{a_l^2}+\frac{z^2}{b_l^2}}} \right]. \tag{B1}$$

We use the superscript '0' to distinguish this function from one we use shortly to model an applied electric field. Agreement with experimental binding energies and hyperfine coupling of the ground state for each donor species, as reported in Tables II and III, sets the best fit values of b and B for each donor. Even though our pseudo wave function is not expected to provide a trustworthy account of the electron state in the central cell, a rough extrapolation to the value of $\Psi(0)$ that is needed to compute the contact hyperfine coupling between the electron and the nucleus can be attained by including a multiplicative bunching factor of Bloch functions at the lattice sites, which estimates the local value of the true wave function at the impurity site[52]. $\eta_{\text{Ge}} \sim 9.5\eta_{Si}$ has been extracted from comparative measurements in Ref. 41, and we use the latest value $\eta_{Si} \approx 159$ as calculated with tight binding

Donor	b (nm^{-1})	B (nm^{-1})	$\epsilon_{A_1}^{exp}$ (meV)[41]	$\epsilon_{A_1}^{th}$ (meV)
P	4.4	25.9	-12.89	-12.96
As	5.8	43.9	-14.17	-13.52
Bi	8.8	69.3	-12.75	-13.26

TABLE II: Fitting of the pseudopotential: the parameters b and B in Eq. A5 are chosen for each donor so that the theoretical ground energy $\epsilon_{A_1}^{th}$ and hyperfine coupling (proportional to $|\Psi(0)|^2_{th}$) match with their experimental values $\epsilon_{A_1}^{exp}$ and A_0.

Donor	A$_0$ (MHz) [41]	$|\Psi(0)|^2_{exp}(cm^{-3})$ [41]	$|\Psi(0)|^2_{th}(cm^{-3})$
P	45.9	0.17×10^{24}	0.19×10^{24}
As	78.0	0.69×10^{24}	0.64×10^{24}
Bi	229	2.15×10^{24}	2.09×10^{24}

TABLE III: Theoretical values are calculated using $|\Psi(0)|^2_{th} = 4\, \eta_{\rm Ge}|F^0(0)|^2$, where $\eta_{\rm Ge} = |u_0(\mathbf{k}_0, 0)|^2/\langle|u_0(\mathbf{k}_0,\mathbf{r})|^2\rangle_{\text{unit cell}} = 9.5\, \eta_{\rm Si}$ as measured in Ref. 41, and $\eta_{\rm Si} = 159.4$ is taken from Ref. 53. F^0 is any of the envelopes $F^0_\mu(0)$, for example that in Eq. 4, since all of them are the same at $\mathbf{r} = 0$

Donor	$\bar{a}_s$ (nm)	$\bar{b}_s$ (nm)	$\bar{\beta}$	$\bar{a}_l$ (nm)	$\bar{b}_l$ (nm)
P	0.666	0.358	1.29	4.69	1.41
As	0.348	0.123	0.597	4.14	1.24
Bi	0.184	0.064	0.318	3.76	1.11

TABLE IV: Wave function parameters for the variationally optimized donor ground state as defined in Eq. (4).

methods in Ref. 53.

We list the optimal parameters of each ground donor wave function, as defined in Eqs. (A2) and (4), in Table IV. Let us remark that different subsets of each valley manifold (e.g. the orbital singlet A_1 and triplet T_2), and of course different orbital states, will require different values for the optimal variational parameters.

Appendix C: Stark physics of Ge-donors

An electric field that is controlled externally can provide a convenient way to control the qubit state: those conditions imply, within our framework, an update of the bulk $[111]$ envelope in Eq.(4) to the new shape quoted in the main text:

$$F_{111} = N\left[\mathrm{e}^{-\sqrt{\frac{x^2+y^2}{a_s^2}+\frac{z^2}{b_s^2}}} + \beta\, \mathrm{e}^{-\sqrt{\frac{x^2+y^2}{a^2_{l,\hat{\mathbf{E}}}}+\frac{z^2}{b^2_{l,\hat{\mathbf{E}}}}}} \right] \times \times (1 + q(\mathbf{E})\hat{\mathbf{E}}\cdot\mathbf{r}). \tag{C1}$$

We are now using an extra variational coefficient $q(\mathbf{E})$ and allow the long range lengths $a_{l,\hat{\mathbf{E}}}$ and $b_{l,\hat{\mathbf{E}}}$ to change from their zero field values. With no further introduction of adjustable parts in our bulk pseudopotential, the effect of the external electric field is non-perturbatively evaluated by repeating the procedure described in the previous Section, for each value of the vector $\mathbf{E}$.

Let us consider the Hamiltonian matrix elements in the valley basis $\{\xi_{111}, \xi_{\bar{1}11}, \xi_{1\bar{1}1}, \xi_{11\bar{1}}\}$: if $\mathbf{E} \parallel \langle 100\rangle$, the field orientation forms equal angles with all valleys, and so the Hamiltonian matrix takes the form $H_{\mu\nu} = \Lambda\delta_{\mu,\nu} + \Delta(1-\delta_{\mu,\nu})$, with $\delta_{\mu,\nu}$ the Kronecker delta function. The diagonal (intra-valley) entries Λ and the off diagonal (inter-valley) couplings Δ are rigidly shifted from their zero-field values, but the overall symmetry of the resulting eigenstates is maintained: in fact, the ground state is still an equal superposition of all valleys, with eigenvalue $\Lambda + 3\Delta$, while the excited states still form a triplet with energy $\Lambda - \Delta$.

At the opposite extreme, if $\mathbf{E} \parallel [111]$, the field orientation makes a maximal distinction between the $[111]$ (aligned 'a') valley and the other three (misaligned 'm') valleys, which results in a Hamiltonian matrix of the form:

$$H = \begin{pmatrix} \Lambda_a & \Delta_a & \Delta_a & \Delta_a \\ \Delta_a & \Lambda_m & \Delta_m & \Delta_m \\ \Delta_a & \Delta_m & \Lambda_m & \Delta_m \\ \Delta_a & \Delta_m & \Delta_m & \Lambda_m \end{pmatrix}, \tag{C2}$$

with $\Lambda_a = \langle\xi_{111}|H|\xi_{111}\rangle$, and, for example, $\Lambda_m = \langle\xi_{\bar{1}11}|H|\xi_{\bar{1}11}\rangle$, $\Delta_a = \langle\xi_{\bar{1}11}|H|\xi_{111}\rangle$, and $\Delta_m = \langle\xi_{\bar{1}11}|H|\xi_{\bar{1}11}\rangle$. The eigensystem now includes two singlets G, E (ground, excited), with energies

$$\epsilon_G^E = \frac{1}{2}\Big(2\Delta_m + \Lambda_a + \Lambda_m \pm |\sqrt{12\Delta_a^2 + (2\Delta_m - \Lambda_a + \Lambda_m)^2}|\Big),$$

and eigenvectors' coefficients

$$\{\alpha_\mu\}_G^E = \frac{(\gamma_G^E, 1, 1, 1)}{\sqrt{3 + (\gamma_G^E)^2}}, \tag{C3}$$

where

$$\gamma_G^E = -\frac{1}{2\Delta_a}\Big[2\Delta_m - \Lambda_a + \Lambda_m \mp |\sqrt{12\Delta_a^2 + (2\Delta_m - \Lambda_a + \Lambda_m)^2}|\Big];$$

and a doublet with intermediate energy $\Lambda_m - \Delta_m$, that is not Stark shifted.

The strong anisotropy of the Ge lowest conduction band ($m^*_\perp \approx 20 m^*_\parallel$) implies that the squeezing of the state ξ_i of each valley will be larger the more orthogonal $\hat{E}$ is to the valley axis. However, the overall Stark effect on the whole wave function results from the interplay of the squeezings of all valleys, each weighted with the coefficients in Eq. (C3).

In the regime of low electric fields relevant to recent experiments[18] ($|\mathbf{E}|$ ~kV/m), the intervalley couplings Δ are

shifted much less than the diagonal valley energies Λ, as they involve higher Fourier components of the linear electric-field term in the Hamiltonian. While all terms will be retained in the numerical calculations that follow, it is instructive to set $\Delta_m \approx \Delta_a \approx \Delta_0$ (Δ_0 being the zero-field intervalley coupling), and acknowledge that owing to the large anisotropy described above $|\Lambda_a - \Lambda_0| \ll |\Lambda_m - \Lambda_0|$ (where Λ_0 the zero field intravalley coupling). If we now expand up to second order in the magnitude of the applied electric field, we find:

$$\epsilon_G(\mathbf{E} \neq 0) - \epsilon_G(\mathbf{E} = 0) \approx \frac{3}{4}(\Lambda_m - \Lambda_a), \quad \text{(C4)}$$

$$\gamma_G(\mathbf{E}) \approx 1 - \frac{1}{4}\frac{[\Lambda_m(\mathbf{E}) - \Lambda_a(\mathbf{E})]}{\Delta_0}. \quad \text{(C5)}$$

The quadratic dependence of these quantities on $|\mathbf{E}|$ is thus made apparent, as linear terms in Λ are forbidden by the parity symmetry within each valley[5]. Furthermore, the reorganization of the valleys that is represented by the coefficient γ_G [see Eq. (C3)] can be now understood as the result of the interplay of the anisotropy of the Ge conduction band, that dictates how the longitudinal and transverse valleys envelopes respond to the applied field within each valley, and the inter-valley coupling Δ_0 (that sets the singlet-triplet energy difference).

1. Hyperfine Stark shifts

For electric fields well below ionization, the relative hyperfine Stark shifts can be parametrized by a single quadratic coefficient η_a, the 'hyperfine susceptibility':

$$\frac{\Delta A}{A_0} = \frac{|\Psi(\mathbf{E} \neq 0, \mathbf{r} = \mathbf{0})|^2}{|\Psi(\mathbf{E} = 0, \mathbf{r} = \mathbf{0})|^2} - 1 \equiv \eta_a E^2. \quad \text{(C6)}$$

Direct substitution of the Stark-shifted donor wave function discussed in the previous section, for different orientations of the applied $\mathbf{E}$, in Eq. (C6) leads to

$$\begin{aligned}
\frac{\Delta A}{A_0}\langle 111\rangle &= \frac{1}{4F_0^2(\mathbf{0})}\frac{1}{3+\gamma_G^2}(3F_{\bar{1}11}(\mathbf{0}) + \gamma_G F_{111}(\mathbf{0}))^2 - 1, \\
\frac{\Delta A}{A_0}\langle 100\rangle &= \frac{1}{F_0^2(\mathbf{0})}F_{111}^2(\mathbf{0}) - 1, \qquad \text{(C7)} \\
\frac{\Delta A}{A_0}\langle 110\rangle &= \frac{1}{4F_0^2(\mathbf{0})}\frac{1}{2+2\gamma_G^2}(2F_{\bar{1}11}(\mathbf{0}) + 2\gamma_G F_{111}(\mathbf{0}))^2 - 1,
\end{aligned}$$

where $F_0(\mathbf{0})$ is the amplitude of any of the envelopes defined in Eq. (4), evaluated at the impurity site.

Our theoretical predictions of the η_a coefficients are reported in Table V for all donors and the three different field orientations considered here. Eqs. (C7) clarify the two different effects of an external field: the envelopes of each valley are renormalized, and the valleys are repopulated as described by the shift of the coefficient γ_G from its zero-field value $\gamma_G = 1$. Both effects, as described by Eqs. (C4) and (C5), give a direct measure of how much the electric field distinguishes between two different valleys. The first effect makes the largest contribution to the total susceptibility η_a, but the second is more responsible for the dependence on the field orientation, which is more pronounced for weaker valley-orbit effects [see Eq. (C5)]. As a consequence, the hyperfine susceptibilities only change mildly with the orientation of the field, but for Ge:P Δ_0 is small enough that η_a can vary by $\sim 10\%$ between different field directions.

Direct comparison of Table V with experimentally obtained parameters for Ge:P and Ge:As donors[18] shows very close agreement in both cases.

The hyperfine susceptibilities we have calculated are about two orders of magnitude larger than those of Si donors. As the bulk hyperfine constants A_0 of Ge:P and Ge:As are about half than the respective Si:P and Si:As donors, and for Ge:Bi it is about five times smaller than in Si:Bi, the absolute hyperfine shifts are 50 or 20 times larger if the same electric field is applied. However, the relevant figure of merit when considering whether hyperfine-shifted Ge donors would make more tunable qubits than those in Si is the maximum shift ΔA that could be attained. As Ge donor wave functions are more spread out in real space, it is expected that they will also more easily completely lose the contact hyperfine coupling, which happens when the field is strong enough that p orbital states, with negligible density at the impurity site, are strongly admixed in the Stark shifted ground state. To determine when this effect comes into play, we can calculate the the Stark shifted $2p$ state can be calculated within the same theory developed here, once a suitable $2p$-like trial envelope is introduced[5]:

$$\Psi^{2p}(\mathbf{r}) = N_p\, z\, e^{-\sqrt{\frac{x^2+y^2}{a_p^2}+\frac{z^2}{b_p^2}}}(1 + q_z^p z). \quad \text{(C8)}$$

We find that the binding energy of the $2p$ manifold for all donors approaches 10 meV, which is close to the $1s_{A1}$ ground states' energy, when the applied field is of the order of 0.2 MV/m. Since the $1s_{A1}$ energies do not move significantly from their bulk value in this regime, at this point the $2p$ orbital manifold will anticross the $1s_{A1}$ state for all donors, and the adiabatic ground state will contain a significant amount of p-character. As a result, for $E \approx 0.2$ MV/m, ΔA will no longer be described by the quadratic susceptibility η_a, but will vary much more strongly with E, giving an unappealing unstable spin energy splitting. Thus, if the qubit states are split by the hyperfine interaction, the maximum stable ΔA that can be achieved with bulk donors are of the order of $0.27 \times (0.2)^2 \times 58.5$ MHz $= 0.63$ MHz (Ge:P), $0.12 \times (0.2)^2 \times 99.3$ MHz $= 0.48$ MHz (Ge:As), $0.17 \times (0.2)^2 \times 292$ MHz $= 1.99$MHz (Ge:Bi), corresponding to maximum ESR frequency shifts of 0.3 MHz, 1 MHz, and 9.5 MHz: these values are curiously very close to those calculated for Si donors in Ref. 5. We conclude that gate times for selective manipulations of spin qubits relying on resonant excitation of locally Stark shifted donors in the bulk are *not* improved from Si to Ge.

Donor	$\eta_a(\mu m^2/V^2)$ (th)			$\eta_a(\mu m^2/V^2)$ (exp)
$\hat{\mathbf{E}}$	$\langle 111\rangle$	$\langle 100\rangle$	$\langle 110\rangle$	
P	-0.27	-0.24	-0.21	-0.22
As	-0.12	-0.1	-0.1	-0.12
Bi	-0.17	-0.17	-0.17	/

TABLE V: Comparison of the theoretical quadratic Stark shift coefficients η_a(th) of the hyperfine couplings of three group V donors in Ge, as calculated from Eq. (C7), and the corresponding experimental values η_a(exp) measured in Ref. 18.

2. Spin-orbit Stark shifts

If an applied electric field is also combined with an external magnetic field, the donor response includes a so-called spin-orbit Stark effect. Following Ref. 54, let us define the **g** tensor as the response of the donor electron spin **S** to some external magnetic field **B**:

$$H_{mag} = \mathbf{S}\cdot\mathbf{g}\cdot\mathbf{B}, \tag{C9}$$

where **g** is averaged over the single-valley g-tensors, with the appropriate weights corresponding to the electron ground state. For a general **B**-orientation angle θ with respect to any valley-axis $\hat{\mu}$, the measured single-valley g_μ-factor is[54]

$$g_\mu^2 \equiv \frac{|\mathbf{g}_\mu\cdot\mathbf{B}|^2}{|\mathbf{B}^2|} = \sum_{i,j}(g_\mu^{ij}B^j)^2/|\mathbf{B}^2| = g_\parallel^2\cos^2\theta + g_\perp^2\sin^2\theta, \tag{C10}$$

where i and j run over the three Cartesian components of the tensors. The overall $\mathbf{g}_0$-tensor in bulk donors is an equal superposition of all the four valley $\mathbf{g}_\mu$-tensors. Experimental measurements in Ref. 41 show that $g_\perp = 1.92 \pm 0.02$, $g_\parallel = 0.87 \pm 0.04$, with relative values across different implanted donor species only varying by a few percent.

In the presence of applied gate voltages or strain perturbations that break the tetrahedral symmetry of the doped crystal, the overall bulk $\mathbf{g} = \sum_\mu \alpha_\mu \mathbf{g}_\mu$ can either be tuned by single-valley modifications of each $\mathbf{g}_\mu$ or by the valley repopulation that reorganizes the α_μ coefficients.[54]. Single-valley g_μ-values can only be shifted by an applied electric field that is not along any $\langle 111\rangle$ crystallographic direction – this was pointed out by Roth[41] and experimentally verified in the same work. In this case, the shift is due to the field enhancing the spin-orbit coupling of other bands to the lowest conduction band. On the other hand, valley repopulation occurs when **E** is not parallel to any $\langle 100\rangle$ direction (i.e. when **E** does not make the same angle with all valleys). The relative importance of these two kinds of orbital coupling can be preliminarily assessed by comparing the energy differences between the respective unperturbed states to be coupled: the inter-band energy difference involved in the single-valley mechanism is two orders of magnitude larger than the $E_{T2} - E_{A1}$ splitting[55] that is relevant for valley repopulation. It is thus predicted that the g-factor shifts will be much larger when the valley repopulation effect plays a role, and this has been indeed verified by *ab initio* calculations in Ge:P[9]. Thus, we limit ourselves to the calculation of the more important spin-orbit Stark shifts induced by valley repopulation; this is anyway necessary since we use a single band approximation which is unable to account for the single valley g-factor shifts. As a consequence, our theoretical predictions aim at describing the full g-factor shift if $\mathbf{E} \parallel \langle 111\rangle$, giving a very tight lower bound if $\mathbf{E} \parallel \langle 110\rangle$, while the smaller shifts in the case $\mathbf{E} \parallel \langle 100\rangle$ cannot be described.

We are now ready to derive Eq. (7) in the main text: if $\mathbf{E} \parallel \langle 111\rangle$, in the Cartesian frame $\{[100],[010],[001]\}$, substitution of the valley coefficients α_μ for the G state from Eq. (C3) gives $\mathbf{g}_{i,j} = \sum_\mu \alpha_\mu \mathbf{g}^\mu_{i,j} = g_0\delta_{i,j} + \Delta_g(1-\delta_{i,j})$, where $g_0 = g_\parallel/3 + 2g_\perp/3$ is the average bulk g-factor, and

$$\Delta_g \equiv \frac{g_\parallel - g_\perp}{3}(\gamma_G^2 - 1)/(3+\gamma_G^2). \tag{C11}$$

The analytical expression for γ_G in Eq. (C5) immediately shows that the spin-orbit Stark shift of bulk donors depends quadratically on **E**. Different directions of the applied magnetic field $\mathbf{B}_0$ will excite different combinations of the **g** tensor components [in the sense clarified by Eq. (C10)].

More quantitavely, we now define the parameter η_g by the following relation:

$$\frac{g(E)}{g(0)} - 1 = \eta_g|\mathbf{E}|^2. \tag{C12}$$

It is a measure of how large the shift with electric field can be when magnetic and electric field and applied in a given geometry. In Table VI we list η_g for various field orientations, and extend our predictions to Ge:As and Ge:Bi. Note that for the $\mathbf{E} \parallel \langle 110\rangle$ configuration there is a smaller valley repopulation and accordingly smaller spin-orbit Stark shifts are predicted.

Our analytical framework highlights clearly the sources of the giant tunability that is also reported in Fig. (1) in the main text: By combining Eqs. (C11) and (C5), we find that Δ_g, which is a measure of the size of the shift, is

$$\Delta_g = \frac{g_\parallel - g_\perp}{3}\frac{\epsilon_G - \epsilon_G^0}{6|\Delta_0|}. \tag{C13}$$

Hence a very large Δ_g is a consequence of the large mass anisotropy in the Ge conduction band [which leads to large $\epsilon_G - \epsilon_G^0$, as seen from Eq. (C4)] and the relatively small valley-orbit couplings Δ_0. In Si donors, the weaker spin-orbit interaction and the smaller anisotropy make the term $g_\parallel - g_\perp$ three orders of magnitude smaller, and a reduction of another order of magnitude comes from the donors being less shallow (as a consequence of larger valley-orbit interaction): this is indeed compatible with measurements in Ref. 28.

Eq. (C13) also clearly shows that $\Delta_g > 0$, since we find that the donor is more bound with increasing magnitude of the applied electric field, but $g_\parallel < g_\perp$, and this is confirmed by the recent measurements of Ge:As in Ref. 18. More remarkably, the agreement between this work and our theory is very good, as shown by Table VI.

Donor	$\mathbf{B}_0$ orientation	$\eta_g^{\rm th}(\mu{\rm m}^2/{\rm V}^2)$		$\eta_g^{\rm exp}$ $(\mu{\rm m}^2/{\rm V}^2)$	
$\hat{\mathbf{E}}$		$\langle 111\rangle$	$\langle 110\rangle$	$\langle 111\rangle$	$\langle 110\rangle$
P	$\mathbf{B}\|\|\mathbf{E}$	0.19	0.1	-	0.09
P	$\mathbf{B}\perp\mathbf{E}$	-0.095	-0.1	-0.13	-
As	$\mathbf{B}\|\|\mathbf{E}$	0.04	0.017	0.04	0.017
As	$\mathbf{B}\perp\mathbf{E}$	-0.02	-0.017	-0.03	-0.012
Bi	$\mathbf{B}\|\|\mathbf{E}$	0.03	0.012	/	
Bi	$\mathbf{B}\perp\mathbf{E}$	-0.015	-0.012	/	

TABLE VI: Comparison of the theoretical quadratic Stark shift coefficients $\eta_g^{\rm th}$ of the g-factors of three group V donors in Ge, as calculated from Eq. (C11), and the corresponding experimental values $\eta_g^{\rm exp}$ measured in Ref. 18.

Appendix D: Two-qubit coupling

We start with some qualitative considerations that are common to exchange coupling calculations across all multi-valley semiconductors. The Heitler-London approximation[30] can give reliable estimates of the exchange splitting $J = E_T - E_S$ between the singlet $|S\rangle = \frac{1}{\sqrt{2}}|\uparrow\downarrow - \downarrow\uparrow\rangle$ and triplet $|T_{0,+,-}\rangle = \frac{1}{\sqrt{2}}|\uparrow\downarrow + \downarrow\uparrow\rangle, |\uparrow\uparrow\rangle, |\downarrow\downarrow\rangle$ spin states of two neutral donors interacting via the Heisenberg antiferromagnetic interaction $J\mathbf{S}_1\cdot\mathbf{S}_2$, with $J>0$ at zero magnetic field. If the overlap between two single-electron wave functions centered at different sites $\mathbf{R}_a, \mathbf{R}_b$, namely $\mathcal{S} = \langle\Psi_a(\mathbf{r}-\mathbf{R}_a)|\Psi_b(\mathbf{r}-\mathbf{R}_b)\rangle$, is small enough, the Heitler-London prescription leads to an estimate of J based on a combination of single and two-particle integrals over the isolated wave functions of the non-interacting system[7,31]. The reliability of such calculations decreases if the overlap is too large, i.e. if the donors are too close. It also fails if the donors are too far apart – $|\mathbf{d} = \mathbf{R}_a - \mathbf{R}_b|$ larger than about 50 effective Bohr radii – where it is found that J can turn negative, thus contradicting the Lieb-Mattis theorem[56]. However, quantum computing goals focus on the intermediate regime, which is a compromise between achieving significant qubit coupling while overcoming the technical difficulties of fabrication very close donors. Thus, the Heitler-London approach has commonly been taken in theoretical predictions of donor couplings in the last fifteen years[5,7,31,32]. The successive advances in understanding and the improvements of calculations of donor couplings have only come from improvements to the theory of the single donor wave function. We remark that all of the integrals contributing to J depend crucially on how the wave function behaves in the spatial region between the two donors, i.e. far enough from the central cell.

The analytical Heitler-London expression for J can be combined into four different terms sharing the same valley structure (as explained in the next Section (S5), and thus showing similar dependences on the donor separation. For the sake of illustration, let us consider the simplest, namely the overlap integral squared $\mathcal{S}^2 = \langle\Psi(\mathbf{r})|\Psi(\mathbf{r}-\mathbf{d})\rangle$:

$$\mathcal{S}^2 = \left(\sum_{\mu,\nu}\alpha_\mu\alpha_\nu\langle\xi_\mu|\xi_\nu\rangle\right)^2 \approx \left(\frac{1}{\#\text{valleys}}\sum_\mu e^{-i\mathbf{k}_\mu\cdot\mathbf{d}}\mathcal{S}_\mu\right)^2 \tag{D1}$$

where $\mathcal{S}_\mu \approx \int d\mathbf{r}F_\mu(\mathbf{r}-\mathbf{R}_a)F_\mu(\mathbf{r}-\mathbf{R}_b)$ is the overlap between envelopes with the same spatial phase, i.e. those pertaining to the same valley. The terms in Eq. (D1) with mixed valleys $\mu\neq\nu$ are suppressed by the large spatial oscillations that come from the phase differences $(\mathbf{k}_{0\mu}-\mathbf{k}_{0\nu})\cdot\mathbf{r}$. In the expression of $\mathcal{S}_\mu$ only the in-phase plane waves of the Bloch functions in Eq. (A2) have been retained, which is again an excellent approximation due to the envelopes not changing significantly over the lengthscale $1/k_0$. Since time-reversal symmetry in the Ge crystal guarantees that $F_\mu = F_{-\mu}$, we can further manipulate Eq. (D1) into

$$\mathcal{S}^2 \approx \frac{1}{(\#\text{valleys})^2}\sum_{\mu,\nu}\cos[(\mathbf{k}_{0\mu}-\mathbf{k}_{0\nu})\cdot\mathbf{d}]\mathcal{S}_\mu\mathcal{S}_\nu, \tag{D2}$$

which highlights the importance of the structure of the conduction band for coupling two spins embedded in multi-valley semiconductors: just like $\mathcal{S}^2$, J will depend on the donor separation $\mathbf{d}$ not only through the smoothly decaying envelope overlaps $\mathcal{S}_\mu$, but also through the highly oscillatory cosine terms whose period is of the order of the crystal lattice constant. Practical implementation of two-qubit operations with uniform control will have to deal with the vast range of coupling magnitudes intrinsic to an ensemble of qubits with different donor separations $\mathbf{d}$.

The first question that we answer in the main text regards the best geometry that shrinks as much as possible this spread of J couplings: It is known[7] that, as explained in Ref. 21, the best option for $\mathbf{d}_0$ in Si is for it to lie along a $\langle 100\rangle$ crystallographic direction. Due to the different band structure in Ge, we find that a different choice of $\mathbf{d}_0$ is optimal. To see this requires considering all the possible sets of $\{(\mathbf{k}_{0\mu}-\mathbf{k}_{0\nu})\cdot\mathbf{d}_0\}_{\mu,\nu=1,2,3,4}$ when $\mathbf{d}_0$ varies across the different crystallographic directions, plus taking into account the role of the anisotropy of the lowest conduction band. In fact, if the envelopes F_μ were spherically symmetric [so that $\mathcal{S}_\mu(\mathbf{r}) = \mathcal{S}_\nu(\mathbf{r})$ for all μ,ν], then the optimal $\mathbf{d}_0$ minimizing the spread of $\mathcal{S}^2$ values in Eq. (D2) for the random misplacements $\mathbf{d}_r$ would be the one that minimizes the sum $\sum_{\mu,\nu=1}^4\cos[(\mathbf{k}_{0\mu}-\mathbf{k}_{0\nu})\cdot\mathbf{d}_0]$. Thus, $\mathbf{d}_0$ should be as close to orthogonal as possible with all of the pairwise differences of valley vectors $\mathbf{k}_{0\mu}$, i.e. it should make equal angles with all valleys and so parallel to $\langle 100\rangle$. However, the very large anisotropy of the Ge conduction band implies that it is better to have as many terms as possible with $(\mathbf{k}_{0\mu}-\mathbf{k}_{0\nu})\perp\mathbf{d}_0$, rather than distributing the orthogonality equally among all terms:[21] this is attained with $\mathbf{d}_0\parallel\langle 110\rangle$.

As a result, in both of the optimal geometries just outlined for Si and Ge, the non-oscillating terms pertaining to valley-differences orthogonal to $\mathbf{d}_0$ make the largest contributions to J. We are thus led to separate our analysis of parallel $\mathbf{d}_r\parallel\mathbf{d}_0$ and orthogonal $\mathbf{d}_r\perp\mathbf{d}_0$ misplacements from the nominal donor separation, since the

qualitative dependence of J is very different in the two cases. As the parallel misplacement is increased, the only effect is a monotonic decrease of the overall coupling due to the weaker overlap of the electronic densities. On the other hand for a fixed parallel displacement, J oscillates markedly as a function of orthogonal misplacement. This is indeed clear from Fig. 4, that shows density plots of J as a function of transverse misplacements for two different fixed parallel misplacements, for both of the ensembles of Si:P and Ge:P donors considered in this work. From our full numerical calculations, we find that to a good approximation it is possible to factor out the effects of parallel and transverse misplacements: $\log[J(\mathbf{d}_r)/J(\mathbf{d}_r = 0)] \approx \log[e^{-1.82(\mathbf{d}_r\cdot\hat{d}_0)/\bar{a}_l}] + \log f(\mathbf{d}_r \wedge \hat{d}_0)$, where $f(x)$ is a highly oscillatory function of its argument.

We reiterate that two sets of J couplings are considered in the main text: the first corresponds to a statistical ensemble of Si:P donor pairs with nominal separation $d_0 = 20$ nm along the [100] crystallographic direction but with random transverse placement error $\mathbf{d}_r$ that is uniformly distributed in the square $[0, \{0, 5\text{ nm}\}, \{0, 5\text{ nm}\}]$, the second to an ensemble of Ge:P donor pairs with nominal separation $d_0 =$ 50 nm along the [110] crystallographic direction and random transverse placement error $\mathbf{d}_r$ that is uniformly distributed in the square of edge length 5 nm in the (110) plane with a vertex at the origin. For symmetry reasons, our analysis is also directly valid for the corresponding squares with edge length 10 nm centered at the origin. If we also include parallel misplacements, we get the full distributions of J-couplings in Si:P and Ge:P for misplacements in the 5-nm cube, which are collected in the histograms in Fig. 2 in the main text. These similar mean couplings correspond to an average donor separation that increases from 20 nm in Si:P to 50 nm in Ge:P. This is compatible with the ratio of the transverse effective Bohr radii in the two materials $\bar{a}_l^{Ge:P}/\bar{a}_l^{Si:P} \approx 2.7$.

We finally remark that the considerations presented in this work do not change if other sets of donor distances are considered: as previously explained, if $\mathbf{d}_0$ is decreased the main effect on J is a simple monotonic exponential gain that is fit well with $J \sim e^{-1.82(\mathbf{d}_0)/\bar{a}_l}$ (which can be compared to the analytical approximate formula in Ref. 57).

Appendix E: Valley structure of the donor spin exchange coupling

We now describe in more detail how we evaluated the exchange coupling between donor and dot using our variational wave functions.

It is convenient to write down the spin exchange splitting between two adjacent donor electrons, evaluated in the Heitler-London approximation[30], in a way that highlights most clearly its valley structure. The latter, in fact, determines predominantly the behaviour of J as a function of the inter-donor separation. If $\Psi(\mathbf{r}_1 - \mathbf{R}_a)$ and $\Psi(\mathbf{r}_2 - \mathbf{R}_b)$ indicate the single-particle electron wave functions of electron 1 and 2, with $\mathbf{r}_i$ defining the electronic coordinates, $\mathbf{R}_j$ the fixed positions of the nuclear pair, and $\mathbf{R}_a - \mathbf{R}_b \equiv \mathbf{d}$, we can write

$$J = \frac{2}{1-\mathcal{S}^4}[\mathcal{S}^2(W + C_D) - C_I + \mathcal{S}\mathcal{T}], \tag{E1}$$

where the single-particle feature W is

$$W = -2\langle\Psi_a|\frac{e^2}{\epsilon_{Si}|\mathbf{r}-\mathbf{R}_b|}|\Psi_a\rangle = -2\langle\Psi_b|\frac{e^2}{\epsilon_{Si}|\mathbf{r}-\mathbf{R}_a|}|\Psi_b\rangle, \tag{E2}$$

the two-particle Coulombic integrals are

$$C_D = \langle\Psi_a(\mathbf{r}_1)\Psi_b(\mathbf{r}_2)|\frac{e^2}{\epsilon_{Si}|\mathbf{r}_1-\mathbf{r}_2|}|\Psi_a(\mathbf{r}_1)\Psi_b(\mathbf{r}_2)\rangle,$$
$$C_I = \langle\Psi_a(\mathbf{r}_1)\Psi_b(\mathbf{r}_2)|\frac{e^2}{\epsilon_{Si}|\mathbf{r}_1-\mathbf{r}_2|}|\Psi_a(\mathbf{r}_2)\Psi_b(\mathbf{r}_1)\rangle, \tag{E3}$$

and

$$\mathcal{T} = -2\langle\Psi_a|\frac{e^2}{\epsilon_{Si}|\mathbf{r}-\mathbf{R}_a|}|\Psi_b\rangle = -2\langle\Psi_a|\frac{e^2}{\epsilon_{Si}|\mathbf{r}-\mathbf{R}_b|}|\Psi_b\rangle. \tag{E4}$$

Now we discuss the qualitative behaviour of each of these quantities in turn. The overlap $\mathcal{S} = \langle\Psi_a|\Psi_b\rangle$ has been already discussed in the main text. W does not oscillate significantly with the inter-donor separation: as a single-particle one-site integral, the interfering valley terms containing $F_\mu(\mathbf{r} - \mathbf{R}_a)F_\nu(\mathbf{r}-\mathbf{R}_a)$ with $\mu \neq \nu$ are much less important than the $\mu = \nu$ ones, which decrease monotonically with increasing d. C_D represents the so-called direct exchange integral, which weights the electron-electron repulsion with the on-site donor densities: as such, it monotonically decreases as the electronic clouds overlap reduces. Unlike the valley structure detailed for the overlap $\mathcal{S}$, the lack of inter-donor integrals prevents the appearance of d-oscillating terms, since

$$\int d\mathbf{r}_1 d\mathbf{r}_2 \left(\sum_\mu u_0(\mathbf{k}_\mu, \mathbf{r}_1 - \mathbf{R}_a)F_\mu(\mathbf{r}_1-\mathbf{R}_a)\cos[\mathbf{k}_\mu\cdot(\mathbf{r}_1-\mathbf{R}_a)]\right)^2 \times \left(\sum_\nu u_0(\mathbf{k}_\nu, \mathbf{r}_2 - \mathbf{R}_b)F_\nu(\mathbf{r}_2-\mathbf{R}_b)\cos[\mathbf{k}_\nu\cdot(\mathbf{r}_2-\mathbf{R}_b)]\right)^2 \approx \frac{1}{4}\int d\mathbf{r}_1 d\mathbf{r}_2 \left(\sum_\mu F_\mu^2(\mathbf{r}_1-\mathbf{R}_a)\right)\left(\sum_\nu F_\nu^2(\mathbf{r}_2-\mathbf{R}_b)\right),$$

where the cosines have been averaged over the integration region, as the lengthscales over which the envelopes vary significantly are much larger than $1/k_0$. Finally, C_I is the indirect exchange integral, which is fundamentally an inter-donor feature, and as such it reproduces the kind of valley pattern underlining the overlap $\mathcal{S}$, but 'squared' for each of the electronic coordinates. After neglecting all spatial terms that oscillate strongly over the integration regions, we can write

$$C_I \approx \frac{1}{(\#\text{valleys})^2}\int d\mathbf{r}_1 d\mathbf{r}_2 F_\mu(\mathbf{r}_1-\mathbf{R}_a)F_\nu(\mathbf{r}_2-\mathbf{R}_b) F_\nu(\mathbf{r}_2-\mathbf{R}_a)\times F_\mu(\mathbf{r}_1-\mathbf{R}_b)\frac{e^2}{|\mathbf{r}_1-\mathbf{r}_2|}e^{i(\mathbf{k}_\mu-\mathbf{k}_\nu)\cdot\mathbf{d}}.$$

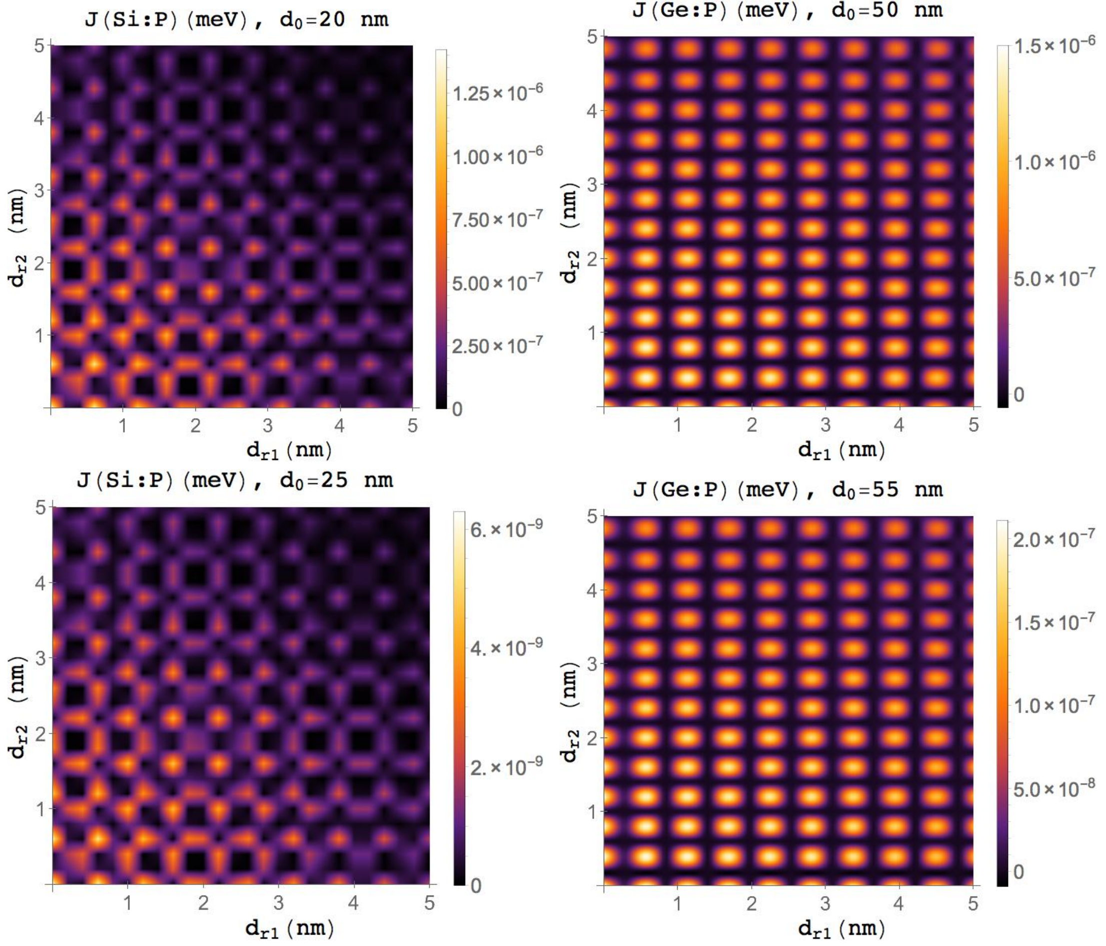

FIG. 4: Density plots of exchange couplings J between neighboring donor spins as a function of misplacements $\mathbf{d}_{r1}, \mathbf{d}_{r2}$ in the plane orthogonal to the nominal donor separation $\mathbf{d}_0$, i.e. $\mathbf{d}_0 = [20 \text{ nm}, 0, 0]$ for Si:P (left) and $\mathbf{d}_0 = [50/\sqrt{2} \text{ nm}, 50/\sqrt{2} \text{ nm}, 0]$ for Ge:P (right). $\{\mathbf{d}_{r1}, \mathbf{d}_{r2}\}$ are sampled with steps of 0.2 nm along each of the two directions; these calculated values are then interpolated for the purpose of illustration. Top panels refer to a situation of no parallel misplacement along $\mathbf{d}_0$, bottom panels have a parallel misplacement of 5 nm. It is clear that the two-dimensional oscillatory pattern is preserved intact between bottom and top pictures, as explained in the text. The period of the oscillations is slightly larger in Si:P, as a result of the different conduction band structure. Remarkably, higher J values survive for longer misplacement vectors in the plane for Ge:P than for Si:P.

Since time-reversal symmetry guarantees that $F_\mu = F_{-\mu}$, we can restate this last result as

$$C_I \approx \frac{1}{(\#\text{valleys})^2} C_I^{\mu\nu}(\mathbf{d}) \cos(\mathbf{k}_\mu - \mathbf{k}_\nu) \cdot \mathbf{d}, \tag{E5}$$

with

$$C_I^{\mu\nu}(\mathbf{d}) \equiv \int d\mathbf{r}_1 d\mathbf{r}_2 F_\mu(\mathbf{r}_1 - \mathbf{R}_a) F_\nu(\mathbf{r}_2 - \mathbf{R}_b) F_\nu(\mathbf{r}_2 - \mathbf{R}_a) \times F_\mu(\mathbf{r}_1 - \mathbf{R}_b) \frac{e^2}{|\mathbf{r}_1 - \mathbf{r}_2|}. \tag{E6}$$

The inter-donor matrix element $\mathcal{T}$ displays essentially the same valley structure as $\mathcal{S}$, as the Fourier transform of the Coulomb potential is not able to couple significantly different valleys $\mu \neq \nu$.

Appendix F: Convergence analysis of our variational method

We now prove the convergence of our variational method to solve the multi-valley EMT equation Eq. 2. Our variational *ansatz* (Eq. 5 in the text) was motivated by the seminal work in Ref. [25], where it was validated after checking that the variational solution to the envelope equation agreed well with the full numerical solution. However, that work focused on describing Si:P, while we are applying our improved framework for the first time to donors in germanium: to check the convergence of our solution we followed the controlled variational method developed by Pendo *et al.* in Ref. [58]. They adopt the Dalgarno-Lewis exact summation method to cross-validate their variational ansatz (See Eq. 32 in Ref.[58]) against an analytical approach to the problem of a Stark shifted doping electron bound in a semiconductor crystal. We accordingly enlarged our variational *ansatz*: for the sake of discussion, again we only focus on the shape of the [111]

envelope, though of course all of the other envelopes have been updated. We define the $\{x, y, z\}$ Cartesian axes along the spatial crystallographic directions $\{[1\bar{2}1], [10\bar{1}], [111]\}$, and with no loss of generality we assume that the electric field lies in the $(x-z)$ plane; then,

$$F_{111} = N\left[\mathrm{e}^{-\sqrt{\frac{x^2+y^2}{a_s^2}+\frac{z^2}{b_s^2}}} + \beta\,\mathrm{e}^{-\sqrt{\frac{x^2+y^2}{a_{l,\hat{\mathbf{E}}}^2}+\frac{z^2}{b_{l,\hat{\mathbf{E}}}^2}}}\right]\times \\ \times\left(1+Q_\perp(\mathbf{E})x+Q_\parallel(\mathbf{E})z\right) \quad \text{(F1)}$$

where $Q_\perp = q_{1,\perp} + q_{2,\perp}\sqrt{\frac{x^2+y^2}{a_l^2}+\frac{z^2}{b_l^2}}$, $Q_\parallel = q_{1,\parallel} + q_{2,\parallel}\sqrt{\frac{x^2+y^2}{a_l^2}+\frac{z^2}{b_l^2}}$, and $q_{1,j}$ and $q_{2,j}$ (for $j = \{\parallel, \perp\}$) are a new larger set of variational coefficients. We repeated all of our calculations with this larger variational basis and checked the convergence of our results. We focus on Ge:P for the sake of discussion: the donor binding energy with an applied electric field, for the range of electric fields that has been investigated in this paper, did not change by more than 1% across all electric field directions. As a consequence, our central cell did not need to be updated. More importantly, the results presented in Table V (the η_A coefficients) did not change by more than 15%: this precision is adequate for the goals of this work, which aims at predicting for the first time the features of quantum gates with spin donors in Ge. Notably, Table V lies at the core of most of the results presented here, since it allows us to compare directly important physical quantities of our donor wavefunction (as discussed in Appendix C) with experimental measurements. The convergence of such results in the face of the enlarging of the variational basis that has just been discussed shows an apparent validation of the effectiveness of our approach to describe the donor wavefunction outside of the central cell - which is key to predicting the features of donor-based quantum gates.

[1] F. A. Zwanenburg, A. S. Dzurak, A. Morello, M. Y. Simmons, L. C. L. Hollenberg, G. Klimeck, S. Rogge, S. N. Coppersmith, and M. A. Eriksson, Rev. Mod. Phys. **85**, 961 (2013).

[2] A. M. Tyryshkin, S. Tojo, J. J. L. Morton, H. Riemann, N. V. Abrosimov, P. Becker, H.-J. Pohl, T. Schenkel, M. L. W. Thewalt, K. M. Itoh, et al., Nat. Mater. **11**, 143 (2012), ISSN 1476-1122.

[3] K. Saeedi, S. Simmons, J. Z. Salvail, P. Dluhy, H. Riemann, N. V. Abrosimov, P. Becker, H.-J. Pohl, J. J. L. Morton, and M. L. W. Thewalt, Science **342**, 830 (2013).

[4] C. Tahan and R. Joynt, Phys. Rev. B **71**, 075315 (2005).

[5] G. Pica, G. Wolfowicz, M. Urdampilleta, M. L. W. Thewalt, H. Riemann, N. V. Abrosimov, P. Becker, H.-J. Pohl, J. J. L. Morton, R. N. Bhatt, et al., Phys. Rev. B **90**, 195204 (2014).

[6] B. E. Kane, Nature **393**, 133 (1998).

[7] B. Koiller, X. Hu, and S. Das Sarma, Phys. Rev. Lett. **88**, 027903 (2002).

[8] F. A Baron, A. A. Kiselev, H. D. Robinson, K. W. Kim, K. L. Wang, and E. Yablonovitch, Phys. Rev. B **68**, 195306 (2003).

[9] R. Rahman, S. H. Park, T. B. Boykin, G. Klimeck, S. Rogge, and L. C. L. Hollenberg, Phys. Rev. B **80**, 155301 (2009).

[10] A. Giorgioni, S. Paleari, S. Cecchi, E. Grilli, G. Isella, W. Jantsch, M. Fanciulli,and F. Pezzoli, ArXiv e-print 1603.08783 (2016).

[11] A. J. Sigillito, R. M. Jock, A. M. Tyryshkin, J. W. Beeman, E. E. Haller, K. M. Itoh, and S. A. Lyon, Phys. Rev. Lett. **115**, 247601 (2015).

[12] R. Vrijen, E. Yablonovitch, K. Wang, H. W. Jiang, A. Balandin, V. Roychowdhury, T. Mor, and D. DiVincenzo, Phys. Rev. A **62**, 012306 (2000).

[13] G. Scappucci, G. Capellini, B. Johnston, W. M. Klesse, J. A. Miwa, and M. Y. Simmons, Nano Letters **11**, 2272 (2011).

[14] M. L. Lee, E. A. Fitzgerald, M. T. Bulsara, M. T. Currie, and A. Lochtefeld, J. Appl. Phys. **97**, 011101 (2005).

[15] T. H. Ning and C. T. Sah, Phys. Rev. B **4**, 3482 (1971).

[16] F. R. Bradbury, A. M. Tyryshkin, G. Sabouret, J. Bokor, T. Schenkel, and S. A. Lyon, Phys. Rev. Lett. **97**, 176404 (2006).

[17] A. Laucht, J. T. Muhonen, F. A. Mohiyaddin, R. Kalra, J. P. Dehollain, S. Freer, F. E. Hudson, M. Veldhorst, R. Rahman, G. Klimeck, K. M. Itoh, D. N. Jamieson, J. C. McCallum, A. S. Dzurak, and A. Morello, Sci. Adv. **1**, 3 (2015).

[18] A. J. Sigillito, A. M. Tyryshkin, J. W. Beeman, E. E. Haller, K. M. Itoh, and S. A. Lyon, Phys. Rev. B **94**, 125204 (2016).

[19] A. G. Fowler, M. Mariantoni, J. M. Martinis, and A. N. Cleland, Phys. Rev. A **86**, 032324 (2012).

[20] J. K. Gamble, N. T. Jacobson, E. Nielsen, A. D. Baczewski, J. E. Moussa, I. Montano and R. P. Muller, Phys. Rev. B **91**, 235318 (2015).

[21] G. Pica, B. W. Lovett, R. N. Bhatt, and S. A. Lyon, Phys. Rev. B **89**, 235306 (2014).

[22] P. Y. Yu and M. Cardona, *Fundamentals of semiconductors* (Springer, 2010).

[23] M. Altarelli, W. Y. Hsu, and R. A. Sabatini, Solid State Phys. **10**, 21 (1977)

[24] M. L. Cohen and T. Bergstresser, Phys.Rev. **141**, 789 (1966).

[25] M. Friesen, Phys. Rev. Lett. **94**, 186403 (2005).

[26] J. Verduijn, G. C. Tettamanzi, and S. Rogge, Nano Letters **13**, 1476 (2013).

[27] G. Wolfowicz, M. Urdampilleta, M. L. W. Thewalt, H. Riemann, N. V. Abrosimov, P. Becker, H.-J. Pohl, and J. J. L. Morton, Phys. Rev. Lett. **113**, 157601 (2014).

[28] A. J. Sigillito, A. M. Tyryshkin and S. A. Lyon, Phys. Rev. Lett. **114**, 217601 (2015).

[29] M. Veldhorst, C. H. Yang, J. C. C. Hwang, W. Huang, J. P. Dehollain, J. T. Muhonen, S. Simmons, A. Laucht, F. E. Hudson, K. M. Itoh, A. Morello,and A. S. Dzurak, Nature **526**, 410 (2015).

[30] W. Heitler and F. London, Z. Phys. p. 455 (1927).

[31] B. Koiller, X. D. Hu, and S. Das Sarma, Phys. Rev. B **66**, 115201 (2002).

[32] C. J. Wellard and L. C. L. Hollenberg, Phys. Rev. B **72**, 085202 (2005).

[33] G. P. Lansbergen, R. Rahman and S. Rogge, Nature Phys. **4**, 656 (2008).

[34] M. Pierre, R. Wacquez, X. Jehl, M. Sanquer, M. Vinet,and O. Cueto Nature Nanotech. **5**, 133 (2009).

[35] M. Fuechsle, J. A. Miwa, S. Mahapatra, H. Ryu, S. Lee, O. Warschkow, L. C. L. Hollenberg, G. Klimeck, and M. Y. Simmons, Nature Nanotech **7**, 242 (2012).

[36] T. Schenkel, C. Lo, C. Weis, A. Schuh, A. Persaud, and J. Bokor, Nucl. Instr. and Meth. in Phys. Res. B **267**, 2563 (2009).

[37] R. Kalra, A. Laucht, C. D. Hill, and A. Morello, Phys. Rev. X **4**, 021044 (2014).
[38] G. Pica, B. W. Lovett, R. N. Bhatt, T. Schenkel, and S. A. Lyon, Phys. Rev. B **93**, 035306 (2016).
[39] S. Nagayama, A. G. Fowler, D. Horsman, S. J. Devitt, and R. Van Meter, noop arxiv.org:1607.00627 (2016).
[40] S. Dushenko, M. Koike, Y. Ando, T. Shinjo, M. Myronov, and M. Shiraishi, Phys. Rev. Lett. **114**, 196602 (2015).
[41] D. K. Wilson, Phys. Rev. **134**, A265 (1964).
[42] R. A. Faulkner, Phys. Rev. **184**, 713 (1969).
[43] A. Baldereschi, Phys. Rev. B **1**, 4673 (1970).
[44] W. Kohn and J. M. Luttinger, Phys. Rev. **98**, 915 (1955).
[45] J. M. Luttinger, andW. Kohn, Phys. Rev. **97**, 869 (1955).
[46] S. T. Pantelides and C. T. Sah, Phys. Rev. B **10**, 621 (1974).
[47] K. Shindo and H. Nara, J. Phys. Soc. Jpn. **40**, 1640 (1976).
[48] A. Debernardi, A. Baldereschi, and M. Fanciulli, Phys. Rev. B **74**, 035202 (2006).
[49] H. T. Hui, Solid State Commun. **154**, 19 (2013).
[50] A. K. Ramdas and S. Rodriguez, Reports on Progress in Physics **44**, 1297 (1981).
[51] R. Resta, Solid State Phys. **10**, L179 (1977).
[52] W.Kohn (Academic Press, 1957), vol. 5.
[53] L. V. C. Assali, H. M. Petrilli, R. B. Capaz, B. Koiller, X. Hu, and S. Das Sarma, Phys. Rev. B **83**, 165301 (2011).
[54] G. Feher, Phys. Rev. **114**, 1219 (1959).
[55] L. M. Roth, Phys. Rev. **118**, 1534 (1960).
[56] D. C. Mattis, *The theory of magnetism made simple* (World Scientific, 2006).
[57] K. Andres, R. N. Bhatt, P. Goalwin, T. M. Rice, and R. E. Walstedt, Phys. Rev. B **24**, 244 (1981).
[58] L. Pendo, E. M. Handberg, V. N. Smelyanskiy, and A. G. Petukhov, Phys. Rev. B **88**, 045307 (2013).